

The fluorescence properties of aerosol larger than 0.8 μm in urban and tropical rainforest locations

A. M. Gabey¹, W. R. Stanley², M. W. Gallagher¹, and P. H. Kaye²

¹Centre for Atmospheric Science, University of Manchester, UK

²Science and Technology Research Institute, University of Hertfordshire, UK

Received: 21 October 2010 – Published in Atmos. Chem. Phys. Discuss.: 7 January 2011

Revised: 13 May 2011 – Accepted: 17 May 2011 – Published: 15 June 2011

Abstract. UV-LIF measurements were performed on ambient aerosol in Manchester, UK (urban city centre, winter) and Borneo, Malaysia (remote, tropical) using a Wide Issue Bioaerosol Spectrometer, version 3 (WIBS3). These sites are taken to represent environments with minor and significant primary biological aerosol (PBA) influences respectively, and the urban dataset describes the fluorescent background aerosol against which PBA must be identified by researchers using LIF. The ensemble aerosol at both sites was characterised over 2–3 weeks by measuring the fluorescence intensity and optical equivalent diameter (D_p) of single particles sized $0.8 \leq D_p \leq 20 \mu\text{m}$. Filter samples were also collected for a subset of the Manchester campaign and analysed using energy dispersive X-Ray (EDX) spectroscopy and environmental scanning electron microscopy (ESEM), which revealed mostly non-PBA at $D \geq 1 \mu\text{m}$.

The WIBS3 features three fluorescence channels: the emission following a 280 nm excitation is recorded at 310–400 nm (channel F1) and 400–600 nm (F2), and fluorescence excited at 350 nm is detected at 400–600 nm (F3). In Manchester the primary size mode of fluorescent and non-fluorescent material was present at 0.8–1.2 μm , with a secondary fluorescent mode at 2–4 μm . In Borneo non-fluorescent material peaked at 0.8–1.2 μm and fluorescent at 3–4 μm . Agreement between fluorescent number concentrations in each channel differed at the two sites, with F1 and F3 reporting similar concentrations in Borneo but F3 outnumbering F1 by a factor of 2–3 across the size spectrum in Manchester.

The fluorescence intensity in each channel generally rose with D_p at both sites with the exception of F1 intensity in

Manchester, which peaked at $D_p = 4 \mu\text{m}$, causing a divergence between F1 and F3 intensity at larger D_p . This divergence and the differing fluorescent particle concentrations demonstrate the additional discrimination provided by the F1 channel in Manchester. The relationships between fluorescence intensities in different pairs of channels were also investigated as a function of D_p . Differences between these metrics were apparent at each site and provide some distinction between the two datasets. Finally, particle selection criteria based on the Borneo dataset were applied to identify a median concentration of 10 “Borneo-like” fluorescent particles per litre in Manchester.

1 Introduction

Primary biological aerosol (PBA) is the subset of the atmospheric aerosol that includes plant and insect debris, fungal and plant spores, pollen, cells, viruses and bacteria. PBA abundance in the atmosphere is poorly constrained and potential feedback on cloud-hydrological pathways is not yet fully included in climate models. Long-range PBA transport has implications for global biodiversity and disease transmission and there are potential effects on cloud microphysical processes because of the ability of PBA to act as “giant” cloud condensation nuclei (GCCN) and heterogeneous ice nuclei (IN) at temperatures as warm as -2°C (Diehl et al., 2001, 2002). In rural areas the PBA is dominated by fungal spores whereas urban locations usually contain a more varied PBA population thought to contain a larger bacterial component (Matthias-Maser and Jaenicke, 1995) because of sources such as municipal waste treatment plants.



Correspondence to: A. Gabey
(andrew.m.gabey@postgrad.manchester.ac.uk)

1.1 PBA fluorescence

Many PBA are fluorescent under ultra-violet illumination because of the presence of intrinsic bio-fluorophores. The absorption cross-section and fluorescence quantum yield of these compounds are large enough that, despite the fact they typically account for $\sim 5\%$ of PBA dry mass (e.g. Faris et al., 1997) their emission dominates the fluorescence from the entire particle. Peaks in PBA fluorescence spectra are often attributable to the co-enzyme NAD(P)H – part of the metabolic process – flavins, and the amino acids, Tryptophan and Tyrosine. The relative strength of these peaks varies between PBA types and sometimes species, allowing some tentative discrimination in the laboratory (e.g. Hill et al., 2009). Tryptophan is excited at wavelengths around 280 nm and emits fluorescence in a peak from 300–400 nm. NADH is excited between 270 and 400 nm and emits between 400 and 600 nm, and Riboflavin is excited at 300–500 nm and emits mostly between 400 and 700 nm (Lakowicz, 2006; Kaye et al., 2005; Hill et al., 2009). The excitation and emission bands of these bio-fluorophores are quite well separated, which allows the detection of fluorescence (which decays rapidly following excitation) to be carried out at the same time as the excitation through the use of optical filters. This technique therefore offers near real-time measurements compared with biochemical analyses, and the ability to monitor concentrations for long periods with no consumables required.

Laboratory measurements (Agranovski et al., 2003a) and field tests (Ho, 1996) using the TSI Ultraviolet Aerodynamic Particle Sizer (UV-APS; 350 nm excitation and 400–600 nm detection) to investigate various bacteria and spores demonstrate that PBA can be detected by UV-LIF at wavelengths corresponding to NAD(P)H, albeit with varying reliability in the case of bacteria. Agranovski et al. also note a higher UV-LIF detection rate compared with using a culturable technique. Discrimination between broad PBA types (e.g. bacteria and fungal spores) is possible when comparing their fluorescence spectra after multiple wavelength excitations (e.g. Sivaprakasam et al., 2004, 2007), although this does not extend to identifying specific biological species. More recently, Pan et al. (2010) used computational processes with data from fluorescence-based detection systems to discriminate PBA from environmental aerosol by comparing the fluorescence spectra of ambient particles with those measured in the laboratory. These proof-of-concept experiments demonstrate the utility of multiple wavelength excitations and post-processing analysis in distinguishing PBA of a given type, but there are few measurements (discussed in Sect. 1.5) of the background aerosol fluorescence that test samples must be distinguished from to reduce false-positive matches.

1.2 Factors affecting PBA fluorescence

In practice several factors affecting PBA fluorescence make it difficult to compare an ambient and a laboratory sample of the same PBA particle. The intensity of NAD(P)H fluorescence from bacteria varies depending on its physiological age, the stage in its lifecycle and environmental stresses such as heat or desiccation (Agranovski et al., 2003b). Biochemical processes within cells also affect the fluorescence quantum yield from fluorophores. One example of this is NADH, which emits higher-intensity fluorescence when bound to proteins (Lakowicz, 2006). Uk Lee et al. (2010) note that ending the biological activity in fungal spores using a thermal shock of 400 °C does not immediately affect their fluorescent intensity when measured with a UV-APS. This demonstrates that it is the breakdown or depletion of bio-fluorophores over longer timescales that affect fluorescence intensity.

The presence of liquid water inside or coating a PBA also affects the measured fluorescence from it. This is noteworthy because pollen (e.g. Diehl et al., 2001), bacterial spores (e.g. Westphal et al., 2003) and fungal spores (e.g. Yarwood, 1950) are known to take up water from their surroundings, even in sub-saturated conditions. Faris et al. (1997) carried out single-particle measurements on aqueous and dry *Bacillus Subtilis* spores and showed that the fluorescence cross-section of wet particles was 25 % lower than for dry particles when UV energy fluence was less than 1.3 mJ cm^{-2} .

1.3 Interferents

Fluorescent non-PBA also exists in the atmosphere, and some possess similar fluorescence properties to PBA. One example is soot, which contains fluorescent Polycyclic Aromatic Hydrocarbons (PAHs). This increases the likelihood of UV-LIF reporting false positives under certain environmental influences. Combustion contributes mostly small aerosol particles that can agglomerate into larger particles comparable in size to PBA. For example, Schauer et al. (2004) note that the PAHs found in $\text{PM}_{2.5}$ material are dominated by fresh local combustion emissions. Humic and Fulvic acids found in soil dust also share these fluorescence properties and are formed during the decomposition of biomass. Aeolian suspension of soil dust favours the coarse mode over smaller particles, providing another source of large fluorescent particles.

1.4 Past direct measurements of ambient PBA

The difficulty associated with counting PBA directly (often using a combination of staining and microscopic techniques) with standard biological samplers means few estimates of total PBA exist in the published literature. A study by Harrison et al. (2005) found concentrations of 35–180 bacteria l^{-1} in urban Birmingham, UK, depending upon

the season. Matthias-Maser and Jaenicke (1995) counted PBA downwind of Mainz, Germany, using optical and electron microscope analyses of filter samples. When the city lay upwind in the spring, bacteria of 0.6–2 μm diameter numbered $\sim 3 \times 10^3 \text{ l}^{-1}$ and dominated the PBA concentration, representing 20–30% of the total aerosol number in this size range and 1–20% at larger sizes. In contrast the rural-influenced PBA was dominated by pollen and fungal spores. The difference between the reported urban bacteria concentrations underlines the difficulty in interpreting total PBA measurements, although they consistently demonstrate that bacteria dominate the PBA number in urban locations. Gilbert and Reynolds (2005) captured and counted fungal spores on glass slides in the understorey of a tropical forest in Queensland, Australia, and found a strong diurnal cycle with concentrations ranging from $\sim 10^2 \text{ l}^{-1}$ in daylight to $\sim 10^3 \text{ l}^{-1}$ at night with a similar, albeit weaker, cycle observed within the canopy.

Many studies use culturable techniques to catalogue the biological species present in the air at a given location, however these do not provide absolute concentrations. Total PBA concentrations have also been inferred using chemical tracers such as Mannitol that are associated with fungal spore ejection. Elbert et al. (2007) perform a comprehensive review of global Mannitol concentrations and derive a fungal spore emission yield of one spore per 5 pg. This carries uncertainties relating to assumptions about the spore size distribution and release mechanism, each of which is dependant upon species. Passively released fungal spores are also not part of these estimates and the result is scaled by a constant value based on the abundance of different fungus species to incorporate them. Bacteria are not described by these tracers but dominate the PBA concentration at remote and high-altitude sites (e.g. Harrison et al., 2005; Bauer et al., 2002), leading to additional uncertainty in PBA number.

1.5 Past fluorescence measurements of ambient aerosol

A small number of published studies of ambient fluorescent aerosol concentrations is now available. Pöschl et al. (2010) characterised the aerosol sized 0.02–10 μm in Amazonia using a range of techniques. A TSI UV-APS and scanning electron microscope measured a size mode at $1.5 \leq D_A \leq 3 \mu\text{m}$ that was dominated by fluorescent PBA. Huffman et al. (2010) performed UV-APS measurements of the ambient aerosol in Mainz, Germany, and report fluorescent size modes at $0.7 \leq D_A \leq 0.9 \mu\text{m}$ and $3 \leq D_A \leq 5 \mu\text{m}$. Fluorescent particles accounted for 20–30% of the total number at $D_A > 3 \mu\text{m}$. They conclude that PAHs are likely to dominate only the sub-1 μm fluorescent size mode.

The continuous fluorescence spectra of individual ambient coarse-mode particles excited at 266 nm (Pinnick et al., 2004; Pan et al., 2007) exhibit a surprising lack of variation, with ten template spectra able to describe more than 90% of the spectra obtained in urban, semi-urban and desert en-

vironments. Fluorescent non-PBA dominates the number of particles sampled at each site, but only short measurements were performed and the size range was limited to $D_A \geq 3 \mu\text{m}$ so the concentration and diurnal behaviour of fluorescent particles is not known.

Gabey et al. (2010) monitored fluorescent particle concentrations using two excitation and detection wavelengths above and below a tropical rainforest canopy in Borneo, Malaysia. They found fluorescent aerosol dominated the total number concentration at 0.8–20 μm with a size mode at 2–3 μm . A strong diurnal concentration cycle was observed below the canopy, peaking at 2×10^3 fluorescent particles l^{-1} , while a similar cycle above peaked at $2 \times 10^2 \text{ l}^{-1}$ suggesting the source was fungal spores, confirmed using ESEM images, generated mainly within the canopy trunk space and in the forest litter zone.

1.6 Scope

This work briefly discusses the possible sources of fluorescent aerosol in Manchester, UK, in December 2009 and compares the characteristics with those recorded within a tropical rainforest in Borneo, Malaysia. The morphology and composition of particles collected on Nuclepore® filters was established using an Environmental Scanning Electron Microscope (ESEM) with energy-dispersive x-ray (EDX) detector. Fluorescent and total particle size distributions were obtained and fluorescence intensity is compared at the two sites to try and find distinctive features. This work is also intended to represent a measurement of the “background” fluorescent aerosol at each site.

Recent work by Pan et al. (2011) used principal component analysis (PCA) to identify the relationships between elastic scattering intensity and within wavelength dispersed fluorescence spectra following 266 and 351 nm excitations. PCA is well-suited to their 44-dimension dataset but this analysis uses only 4 (3 fluorescence + D_p) so a more conventional analysis of the relations between fluorescence in different channels and D_p is therefore presented.

2 Methods and instrumentation

2.1 Wide-Issue Bioaerosol Spectrometer version 3 (WIBS3)

The WIBS3 (Kaye et al., 2005; Foot et al., 2008) performed single-particle UV-LIF measurements at each site. Air flows through the instrument at 2.38 l min^{-1} with 10% drawn through a tube of 1.2 mm inner diameter to produce a single-file stream of aerosol through the centre of a sensing region. The remainder of the air is filtered and re-introduced as a sheath flow. A particle passing through the sensing region encounters a 632 nm diode laser beam and the intensity of light elastically scattered forward and sideways is measured to estimate particle diameter from a 2-D lookup

table based on a Mie scattering model. Single-particle size is sorted into one of 11 bins chosen based on the instrument response to calibration particles in the laboratory. The total WIBS3-reported concentration is comparable to that of a Grimm Inc. Dust Monitor 1.108 at $D_p \geq 0.8 \mu\text{m}$ in Manchester. Optical equivalent diameter is influenced by particle refractive index (composition effects) and diffraction (morphological effects) and peaks in the size spectrum are consequently broadened when a number of sources influence the aerosol at a site.

Two optically filtered Xenon flash-lamps sequentially provide excitations centred at wavelengths of $280 \pm \sim 20 \text{ nm}$ and $350 \pm \sim 50 \text{ nm}$ with an energy fluence of $320\text{--}350 \mu\text{J cm}^{-2}$. Two spherical mirrors, each subtending 1.33 steradian, focus any fluorescence onto one of two photomultiplier tubes (PMTs), each optically filtered to limit their wavelength response to one of two bands that do not overlap the excitation emissions: 310–400 nm and 400–600 nm. The recorded fluorescence intensity for each particle is not an absolute value and is therefore stated in arbitrary units (a.u.). The intensity scale is different between channels but does not change between campaigns based on the unchanged instrument response to fluorescent and non-fluorescent calibration particles in the intervening period.

Both PMTs record fluorescence during the 280 nm excitation because no detection bands overlap the excitation band, however only the 400–600 nm PMT operates during the 350 nm excitation. The excitation and detection wavelengths were chosen to correspond to the excitation and fluorescence wavebands of Tryptophan and NAD(P)H.

2.2 Electron microscopy and elemental analysis of filter samples

To supplement the Manchester WIBS3 data, a portable PM₁₀ sampler (SKC, Inc.) was operated on several arbitrarily selected days in order to capture each part of the diurnal cycle. Aerosol was collected onto NuclePore® substrates (pore size 400 nm) at 71 min^{-1} for a total of 26 h over three days. ESEM (Philips XL30 ESEM-FG) was used to image the particles on the substrates. Unlike conventional SEM, ESEM uses a lower vacuum with gaseous H₂O inside the imaging chamber so that the samples do not need to be coated before imaging. Each filter section was fixed onto an aluminium stub using double-sided carbon film. Secondary electron images were collected using the gaseous secondary electron (GSE) detector in low-vacuum (“environmental”) mode (H₂O pressure = 0.5 Torr).

Elemental analysis of each particle was performed using the EDX spectrometer attached to the ESEM. This uses a 15 keV electron beam to liberate an electron from the “K” shell of each atom in a sample. The X-ray emission associated with the subsequent electronic transition has an energy characterised by the atomic species and this yields

an energy spectrum with peaks corresponding to the most common elements in the sample.

2.3 Data processing and particle selection criteria

A minimum fluorescence intensity threshold is applied to WIBS3 data to remove low-level fluorescence effects from internal components. This is discussed in detail in Gabey et al. (2010) and is likely to misclassify $\sim 0.5\%$ of non-fluorescent particles as fluorescent in each channel. The threshold is subtracted before any comparisons of fluorescence intensity are made.

If a second particle passes through the WIBS3 sensing region within $\sim 10 \text{ ms}$ of the first it is not classified because of the dead-time associated with the Xenon lamps. The second particle is instead recorded as “missed” by the laser particle detection system. Approximately 10% of all particles were missed at each site, and this information is used to scale the fluorescent and non-fluorescent number concentrations, which are calculated at 15-min intervals in this analysis.

A minimum elastic scattering pulse duration and intensity threshold are set to stop the WIBS3 counting brief noise spikes as aerosol particles. This threshold was raised from its default value (that used in Borneo) in Manchester because of transient rises in the noise floor each lasting $\sim 1 \text{ min}$ that led to large numbers of nonexistent “0.3–0.5 μm particles” triggering the Xenon lamps at their maximum rate. No particles in this size range were reported under normal circumstances therefore these events are readily identified and excluded accordingly. This affected $< 1\%$ of the Manchester dataset, but the counting efficiency was reduced between these events because of the more stringent criteria being applied. Comparisons with another OPC (Grimm Inc. Dust Monitor 1.108) show that the maximum reduction in counting efficiency is 50% at $0.8 \leq D_p \leq 1 \mu\text{m}$, 20% at $1 \leq D_p \leq 1.6 \mu\text{m}$ and is negligible for larger particles.

Seven different particle categories are specified in the analysis, based on whether or not fluorescence is observed in each channel, and these are listed in Table 1. This includes the total number concentration (N_{TOT}) and particles with fluorescence detected in each of the three channels (N_{F1} , N_{F2} and N_{F3}). Particles exhibiting fluorescence in pairs of channels ($N_{1 \text{ AND } 3}$, $N_{2 \text{ AND } 3}$ and $N_{1 \text{ AND } 2}$) are also resolved to complement a discussion of fluorescence intensity ratios. Fluorescence spectra published by other researchers (e.g. Pinnick et al., 1998; Sivaprakasam et al., 2004) show that fungal spores often exhibit broad fluorescence peaks (corresponding to WIBS3 channels F1 and F3), bacteria often features a distinct 300–400 nm peak (F1) and some bacteria emit a broader fluorescence spectrum (triggering F1 and F2). The F1 and F3 channels respectively comprise excitation and detection bands designed to target Tryptophan and NADH, although fluorescence in these channels is not unique to these molecules or even to PBA.

Table 1. The fluorescent and non-fluorescent particle types specified in the analysis.

Short name	Description
TOT	Total number concentration
NON	No fluorescence detected in any channel
F1	Fluorescence detected in channel F1 (excitation at 280 nm, detection 310–400 nm)
F2	Fluorescence detected in channel F2 (excitation at 280 nm, detection 400–600 nm)
F3	Fluorescence detected in channel F3 (excitation at 370 nm, detection 400–600 nm)
F1 AND 3	Fluorescence present in F1 and F3 (the “FBAP” criterion in Gabey et al., 2010)
F1 AND 2	Fluorescence present in F1 and F2
F2 AND 3	Fluorescence present in F2 and F3

Some particle fluorescence is intense enough to saturate the detection channel. These particles are included in fluorescent number concentrations but excluded from the subsequent discussion of fluorescence intensity because they would produce non-physical results. The contribution of saturating particles ranged from 0.008 % to 3 % of N_{TOT} in the size range $0.8 \leq D_p \leq 20 \mu\text{m}$, with a higher incidence of saturation among larger particles. A summary of saturating particle abundance is printed in Table S1 as a percentage of N_{TOT} and fluorescent number concentration. The greatest proportion was found in the F1 channel in Borneo, where they accounted for more than 20 % at $D_p \geq 8 \mu\text{m}$, and their impact on the analysis is noted where appropriate.

2.4 Site descriptions

Manchester is a medium-sized city (estimated population 483 000 – Manchester City Council, 2009) in the North-West of England. The WIBS3 and filter sampler were located 15 m above ground level on a measurement platform at the Centre for Atmospheric Science, University of Manchester. Data was collected from the 4–21 December 2009. The building is situated approximately 1 km from the centre of Manchester, 50 metres from Oxford Road (a main traffic route to and from the city centre). A number of small parks and greens lay 1–2 km from the university, and extensive heath land is present beyond 15 km to the West of the city centre.

Tropical rainforest data was collected in Danum valley, N.E. Borneo, from June–July 2008 as part of the second OP3/ACES intensive campaign (a project overview is available in Hewitt et al., 2010) at a site around 60 km west of the nearest town (Lahad Datu). The WIBS3 inlet was situated 2 m above the forest floor, around 30 m beneath the canopy. Three weeks of data was obtained, and the nature of the fluorescent aerosol is discussed in Gabey et al. (2010). The forest floor is thought to represent an environment rich in fungal spores in the afternoon and evening, with higher non-biological aerosol concentrations present in the middle of the day.

3 Results and discussion

3.1 Size distribution and number concentration of fluorescent particles

3.1.1 Manchester WIBS results

The time series of N_{TOT} (upper panel) and N_{F1} , N_{F2} and N_{F3} (lower panel) are plotted in Fig. 1 with shaded areas that represent periods when the filter sampler was running. Throughout December N_{NON} is an order of magnitude larger than any of the fluorescent concentrations, at $900\text{--}21001^{-1}$. N_{F1} is typically $0\text{--}1001^{-1}$, N_{F2} is typically $0\text{--}2001^{-1}$ and N_{F3} is typically $0\text{--}3001^{-1}$, with these “typical” values representing the 10th and 90th percentiles during the respective periods. Elevated number concentrations also occur on several days, during which N_{F3} exceeds 10001^{-1} and N_{F2} and N_{F3} are also strongly enhanced for 1.5 days from the 10–12 December.

Data coinciding with filter collections are summarised by a box-and-whisker plot in Fig. 2i with the plots for the overall dataset in Fig. 2ii. Median N_{NON} is smaller during filter sampling periods and the median fluorescent number concentrations are larger. Both of these changes are within their respective inter-quartile ranges but amount to a doubling in the fluorescent number fraction during filter sampling. N_{F1} , N_{F2} and N_{F3} represented 5 %, 10 % and 19 % of N_{TOT} respectively during filter sampling periods whereas these figures reduce to 3 %, 6 % and 11 % of N_{TOT} when the entire dataset is used. The enhanced number fractions manifest as an increase across the size spectrum (not shown) rather than in a particular size interval. The filters therefore represent higher than average concentrations for December, but such events are not unique in this dataset and they are concluded to be broadly representative of the material found in Manchester during December 2009.

Large variations in N_{TOT} and fluorescent concentrations take place each day in Manchester, and Fig. 3 shows the diurnal cycles of each particle type. N_{NON} is greatest between 05:00–10:00 and 17:00–19:00, and each fluorescent concentration peaks strongly at 09:00–10:00 with a rapid falloff in N_{F2} and N_{F3} but a more gradual reduction in N_{F1} thereafter.

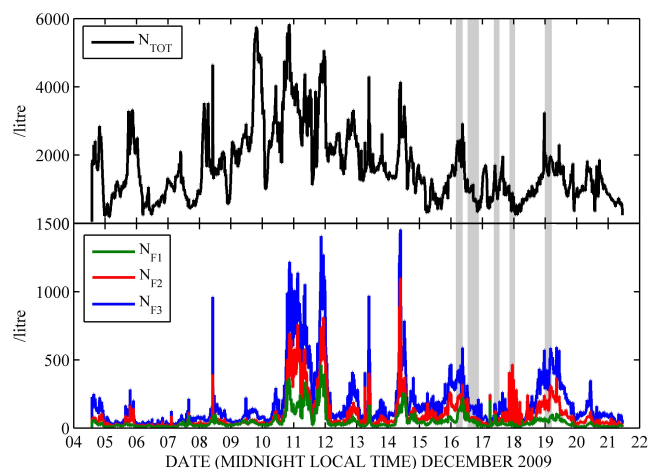


Fig. 1. Time series of WIBS3 number concentrations in Manchester 2009. Filter samples were collected in the periods marked by shaded areas.

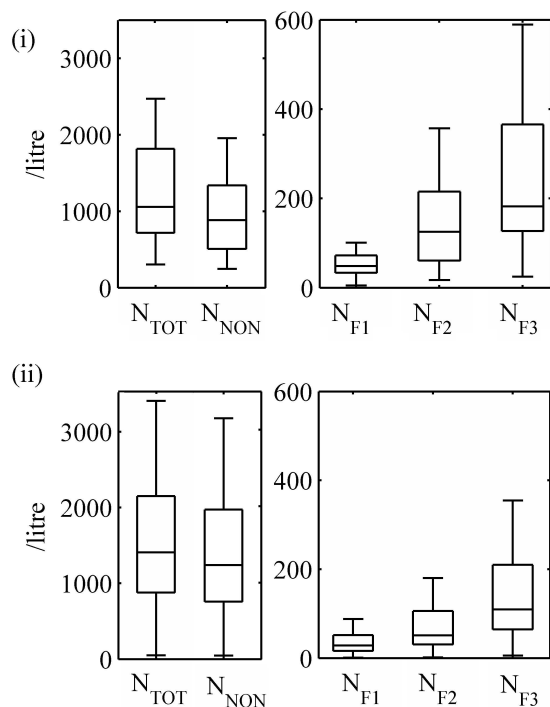


Fig. 2. Box-and-whisker plots of N_{NON} , N_{TOT} and fluorescent number concentrations in Manchester during (i) filter sampling periods and (ii) for the overall dataset.

The fact that fluorescent number concentrations increase in the same period as N_{NON} means traffic activity cannot be ruled out as a fluorescent particle source, either through re-suspension of PBA or production of PAHs. Small rises in N_{F2} and N_{F3} (but not N_{F1}), also occur through the afternoon and peak at $\sim 20:00$.

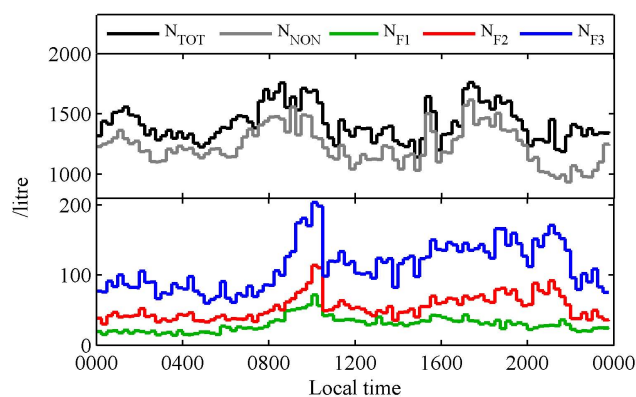


Fig. 3. Diurnal (median) variation in fluorescent, non-fluorescent and total number concentrations in Manchester.

Number size distributions ($dN/d\log D_p$) of each particle type in Manchester are plotted in Fig. 4, along with the median number fraction N/N_{TOT} . Throughout the measurement period N_{NON} (Fig. 4v) dominates N_{TOT} (Fig. 4i) and both size distributions peak at $1.2 \mu\text{m}$. This peak is not explicitly reported by particle counters sensitive to broader size ranges and is the manifestation of increasing aerosol concentration with decreasing D_p in WIBS3 data. Its appearance at $1.2 \mu\text{m}$ rather than $0.8 \mu\text{m}$ is a combination of the increasing WIBS3 counting efficiency at $0.5\text{--}1 \mu\text{m}$, its D_p estimates of material sized $0.8\text{--}1 \mu\text{m}$, and the fact that each size distribution is plotted to the logarithmic mid-bin.

The N_{NON} number fraction reduces with size and reflects how fluorescent particles dominate at $D_p \geq 6 \mu\text{m}$. Each fluorescent number distribution N_{F1} , N_{F2} and N_{F3} (Fig. 4ii–iv) contains a primary size mode at $1.2 \mu\text{m}$ and a secondary mode at $1.5 \leq D_p \leq 3 \mu\text{m}$ which is around half the strength, and not present in the N_{NON} distribution. The primary fluorescent size modes in N_{F1} , N_{F2} and N_{F3} respectively account for 1.3 %, 2.5 % and 5 % of N_{TOT} . These are greater than the misclassification likely to arise from the fluorescence thresholding process, and the fluorescent number fractions generally increase with particle size, peaking at $8\text{--}10 \mu\text{m}$ with values of 20 %, 60 % and 80 % respectively. The size distributions of particles exhibiting fluorescence in each combination of F1, F2 and F3 in Manchester are plotted in Fig. S1 and feature prominent modes at $2\text{--}4 \mu\text{m}$, with weaker features at $1.2 \mu\text{m}$.

3.1.2 Electron microscope analysis of filter samples

To gain an impression of the range of particle sources in Manchester, 105 particles with diameters larger than approximately $1 \mu\text{m}$ were chosen manually for imaging and EDX analysis, with an emphasis on finding different morphologies. A further 50 particles were imaged without EDX analysis and revealed two further PBA candidates. The largest signal peaks in the EDX spectra collected usually corresponded to the elements Al, C, Ca, Cl, Fe, O, S and Si.

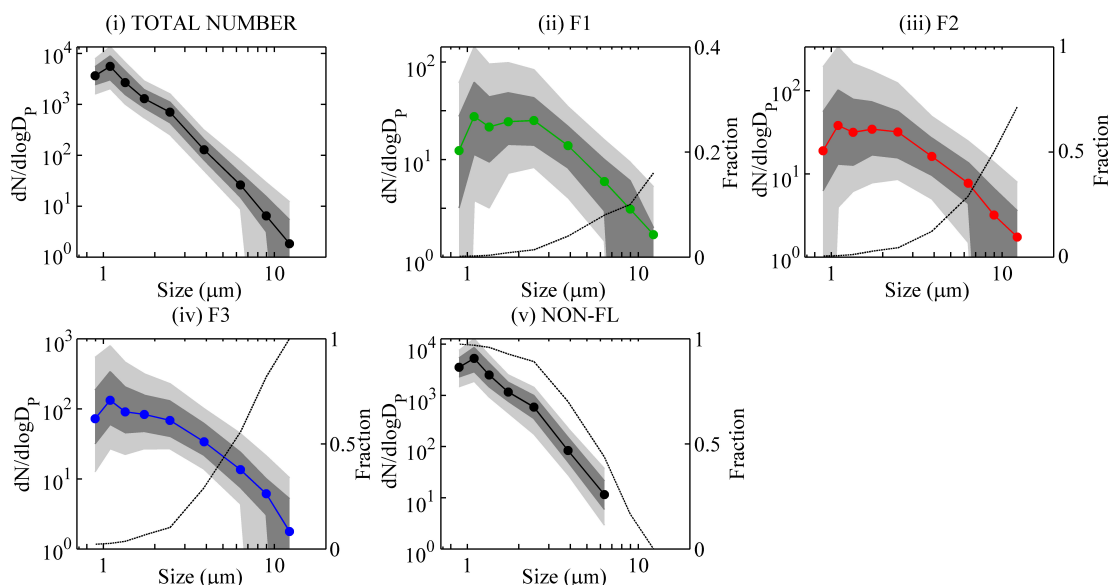


Fig. 4. Manchester number size distributions (logarithmic mid-size bins) for each particle type. Solid line: median, dark shading: interquartile range light shading: 10% and 90%. Dashed lines show median number fraction N/N_{TOT} . Percentiles intersecting the x-axis represent a zero concentration.

As a basic classification scheme the relative height of these peaks was recorded and the particles sorted into basic classes based on the largest peak. If the second largest peak height was more than 50% of the first, the particle was classed as a “mixed” type. A selection of the most common electrographs and the PBA candidates is presented in Fig. S9. The abundance of each class is displayed as a pie chart in Fig. 5, with Carbon, Calcium, Silicates and Iron Oxide dominating the collected spectra. The recorded images show that the carbon-rich particles are dominated by soot across the size range 1–10 μm , with the notable exception of three particles sized 3–5 μm that appear to be PBA.

Based on this information the majority of ambient coarse-mode aerosol in Manchester is derived from a combination of anthropogenic sources, dust transport and sea-salt, with only a minor role for PBA. A quantitative result from this analysis cannot be inferred because of uncharacterised particle losses, the small sample size and a manual selection process biased towards maximising the range of particle morphologies. The results are, however, consistent with previous work performed at an urban roadside location in Birmingham, UK, by Harrison et al. (2004). The presence of what appear to be soot agglomerates throughout the size spectrum raises the possibility of fluorescent non-PBA from combustion aerosols being detected by the WIBS3 in Manchester. Borneo ESEM images (<http://www.atmos-chem-phys-discuss.net/9/C8501/2009/acpd-9-C8501-2009.pdf>) for Gabey et al. (2010) feature a large proportion of structural units bearing little resemblance to the images obtained in Manchester. A more detailed discussion of the likely nature of the Manchester aerosol is presented in Sect. 4.

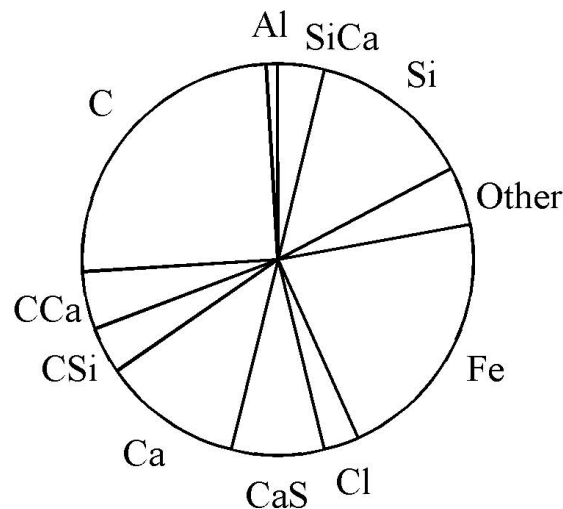


Fig. 5. The proportion of EDX spectra dominated by one or two elements.

3.1.3 Borneo WIBS3 results

We have further examined the data collected in a tropical rainforest in Borneo, Malaysia. This dataset is concluded by Gabey et al. (2010) to represent an environment where N_{TOT} is dominated by PBA. The time series of N_{TOT} , N_{NON} and fluorescent number concentrations found beneath the canopy are printed in Fig. 6. A strong fluorescent particle diurnal behaviour dominates N_{TOT} , and both N_{F1} and N_{F3} peak at $1000\text{--}2000\text{ l}^{-1}$ each day through a series of regular transient

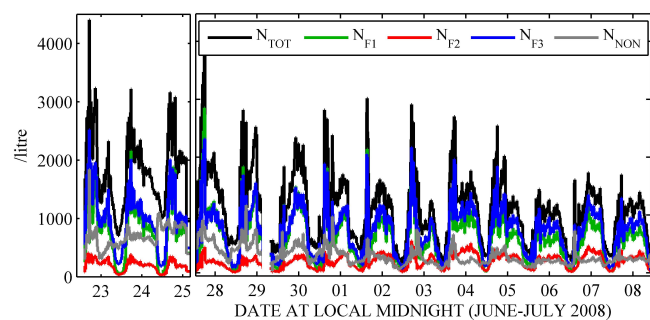


Fig. 6. Time series of WIBS3 Borneo number concentration, adapted from Gabey et al. (2010).

spikes that begin at 15:00 and lead to elevated concentrations through the evening. These features are also present in N_{F2} , which peaks at 300–400 l^{-1} . The similarity between N_{F1} and N_{F3} occurs because the majority of particles exhibit fluorescence in both channels. The concentration of fluorescent material reaches its minimum of $\sim 50 \text{l}^{-1}$ during the mid-morning. In contrast, N_{NON} remains constant or increases so that it dominates N_{TOT} in the same period.

The size distribution and number fraction of each Borneo particle type is printed in Fig. 7. N_{TOT} (Fig. 7i) is dominated by a strong mode at 2–3 μm with a weaker mode at 1.2 μm . The N_{NON} size distribution (Fig. 7v) peaks at 1.2 μm , accounting for 80 % of N_{TOT} at this size. Two N_{NON} events appear in the time series each day: a midday peak thought to be related to material entrained through the canopy and a mid-afternoon peak of non-fluorescent material correlated with the PBA concentration spikes. The former contributes N_{NON} sized 0.8–1.2 μm and the latter contributes N_{NON} with D_p up to 4 μm . The N_{NON} number fraction is also enhanced at 9 μm and the fluorescent number fraction therefore plateaus at large D_p .

The 2–3 μm N_{TOT} mode consists mostly of fluorescent material, with N_{F1} and N_{F3} (Fig. 7ii, iv) accounting for 60 % and 80 % of N_{TOT} at this size range. Supplementary size distributions of particles with fluorescence in each pair of channels are printed in Fig. S2 (Supplement). Like N_{F1} and N_{F3} , $N_{F1 \text{ AND } 3}$ (Fig. S2iii) is 60 % at 2–3 μm , highlighting the overlap between these two metrics. N_{F2} peaks at 4 μm rather than 3 μm , probably because the measured fluorescence intensity in channel F2 (I_{F2}) is lower than both I_{F1} and I_{F3} , which has implications for the fluorescent particle detection rate at smaller sizes. The fluorescent number fractions all increase with D_p , with N_{F1} and N_{F3} (and therefore $N_{F1 \text{ AND } 3}$) accounting for 100 % of the few particles larger than 10 μm .

3.1.4 Comparison of the size spectra between sites

The number concentration and size distribution of fluorescent particles in Manchester and Borneo differ significantly: N_{F1} and N_{F3} are comparable in Borneo and primarily oc-

cupy a 2–4 μm size mode whereas in Manchester the primary mode is at 0.8–1.2 μm and N_{F1} and N_{F3} differ by a factor of 2–3 in favour of N_{F3} . In Borneo N_{F2} is around 25 % of N_{F1} but N_{F2} consistently exceeds N_{F1} in Manchester. One surprising feature in the Manchester dataset is that while all particles larger than 9 μm are fluorescent, few emit in multiple detection channels.

Both Manchester and Borneo have a contribution of fluorescent material in all three channels at $D_p > 1.6 \mu\text{m}$ and the largest particle sizes are dominated by fluorescent material. This implies a significant ambiguity in ability to ascribe fluorescence solely to PBA because of the likelihood that non-PBA contribute in Manchester.

3.2 Fluorescence intensity at each site

For the purposes of this analysis, the Borneo dataset is taken to represent a generic PBA population dominated by multiple fungal spore species released shortly before detection and therefore largely unperturbed by the environmental conditions. Histograms of fluorescence intensity at each site (with minimum thresholds subtracted) are printed in Fig. S3. Each distribution is mono-modal in the lower 25 % of the instrument dynamic range, with contributions along the entire detection range at both sites. I_{F1} peaks in the lowest intensity interval in Manchester but exhibits a clear mode at higher intensity in Borneo. I_{F2} and I_{F3} are consistent at both sites, with each peaking close to the minimum threshold. These similarities and the lack of features in each curve render setting a range of fluorescent intensities to distinguish between the aerosol at the two sites difficult without invoking particle diameter or additional dimensions.

Histograms of fluorescence intensity divided by elastic scattering intensity may produce unique results at each site because of the differing size spectra but similar fluorescence intensity distributions. The distributions of this quantity in each channel (denoted by square brackets) are shown in Fig. S4. The $[I_{F1}]$ and $[I_{F3}]$ plots are similar at each site with overlapping full width half maxima and ranges, whilst less overlap is present in $[I_{F2}]$, allowing unique ranges to be specified. If this was adopted as a classification scheme, however, N_{F1} and N_{F3} at the two sites could only be distinguished using D_p , which itself is not an independent degree of freedom because it is based on elastic scattering intensity.

The linear relationship between fluorescence intensity of a homogeneous fluorescent population and particle cross-sectional area was reported by Hill et al. (2001). Investigating the dependence of measured fluorescence intensity on D_p offers more complete information on the homogeneity of the aerosol population because this retains D_p as a degree of freedom. This approach also allows discontinuities that might indicate different fluorescent particle species to be visualised readily. Plots of I_{F1} , I_{F2} and I_{F3} versus D_p are shown in Fig. 8i–iii for Borneo and Fig. 8iv–vi for Manchester. With the notable exception of I_{F1} in Manchester, these

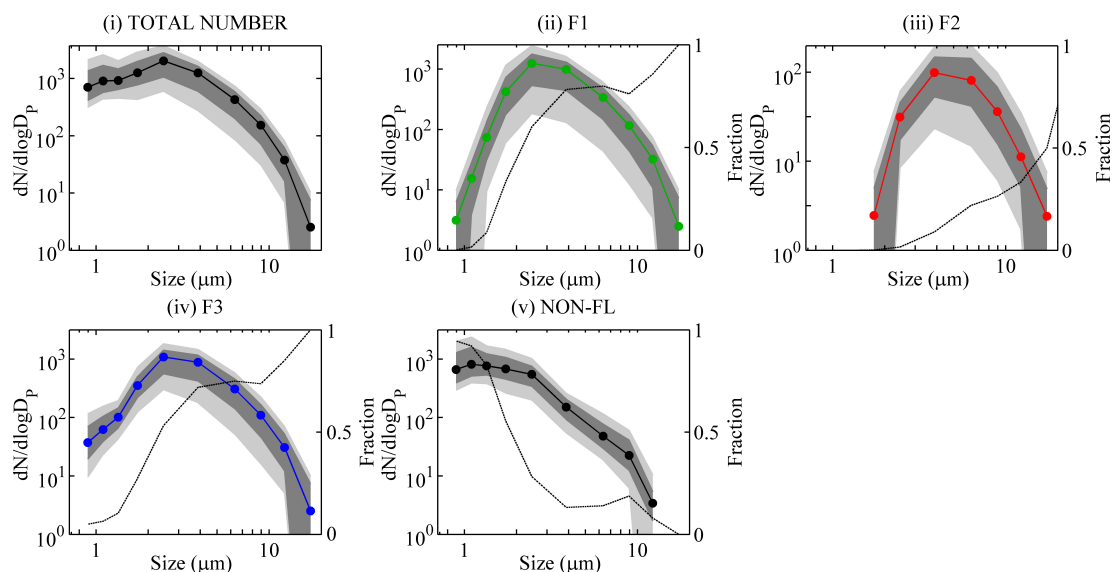


Fig. 7. Borneo number size distributions (logarithmic mid-size bins) for each particle type. Solid line: median, dark shading: inter-quartile range light shading: 10 % and 90 %. Dashed lines show median number fraction N/N_{TOT} . Percentiles intersecting the x-axis represent a zero concentration.

curves each feature a positive trend between intensity and D_p between 0.9 and 10 μm . A much narrower inter-quartile range of I_{F2} and I_{F3} was observed in each size interval in Borneo compared with Manchester, and a number of features are unique to each site.

I_{F1} (Fig. 8i) rises steadily in the interval $0.8 \leq D_p \leq 4 \mu\text{m}$ at both sites, and decreases at $D_p \geq 4 \mu\text{m}$ in Manchester. A similar initial rise in Borneo I_{F1} (Fig. 8iv) continues at $D_p \geq 4 \mu\text{m}$ and a plateau is reached at 7 μm . The former appears to be a feature of the urban aerosol and the latter is likely the result of saturating particles being excluded. The reduction in Manchester I_{F1} is consistent with the lack of dual-channel fluorescence from particles larger than 6 μm in Manchester (Fig. S1) and the divergence between I_{F1} and I_{F3} at $D_p > 4 \mu\text{m}$ is interesting because this observation is contrary to those in the other channels at both sites, and demonstrates a 10 μm particle that exhibits comparable fluorescence intensity to a 1 μm particle despite its surface area being 100 times greater. This suggests a far smaller fluorophore concentration or the presence of optically absorbing material in this particle “species”. It should be classed separately for either reason.

The variation of I_{F2} (Fig. 8v) is distinct from that of I_{F1} and I_{F3} in Borneo because it features an enhancement at 0.8–1.2 μm in which 10 % of particles emit fluorescence as intense as that from 2–3 μm particles. It is likely these are of a different type to their larger counterparts and this was not established in Gabey et al. (2010). The upper limits of recorded Borneo I_{F2} are low compared with other channels and this may account for the relatively small N_{F2} .

There is no Borneo I_{F3} enhancement at 0.9–1.2 μm corresponding to that in I_{F2} (Fig. 8v), therefore it is either rare amongst N_{F3} or dependant upon excitation wavelength. Hill et al. (2009) note that excitation wavelengths shorter than 315 nm are required to induce fluorescence in water-borne bacterial cells, and airborne bacteria of $\sim 1 \mu\text{m}$ diameter are not uncommon according to work in various environments by Matthias-Maser et al. Whilst this is a possible explanation for the feature in the Borneo understorey, the fluorescence spectra of bacteria frequently feature a strong Tryptophan emission, which would produce a 1.2 μm feature in the N_{F1} AND 2 size distribution (Fig. S2i), but this peaks at 2–4 μm and no sub-2 μm particles of this type were detected.

The linearity between I_{F2} and I_{F3} and D_p is also surprising in light of the Hill et al. (2001) study and points to a mixture of subtly different fluorescent particle types in each size interval. A version of Fig. 8 using a linear scale is shown in Fig. S10 to highlight this. It should also be noted that similar inter-quartile ranges of intensity are obtained when data from a single day is analysed, therefore the large range is not an artefact of long datasets.

3.3 Fluorescence intensity in different pairs of channels

The relationships between I_{F1} , I_{F2} and I_{F3} can be characterised more formally than in the previous section by calculating the ratio and correlation coefficient r between single-particle fluorescence intensities in pairs of channels. Those particles exhibiting fluorescence in two detection channels were selected and the ratio of intensity in both was calculated as a function of D_p . Classification based on these ratios

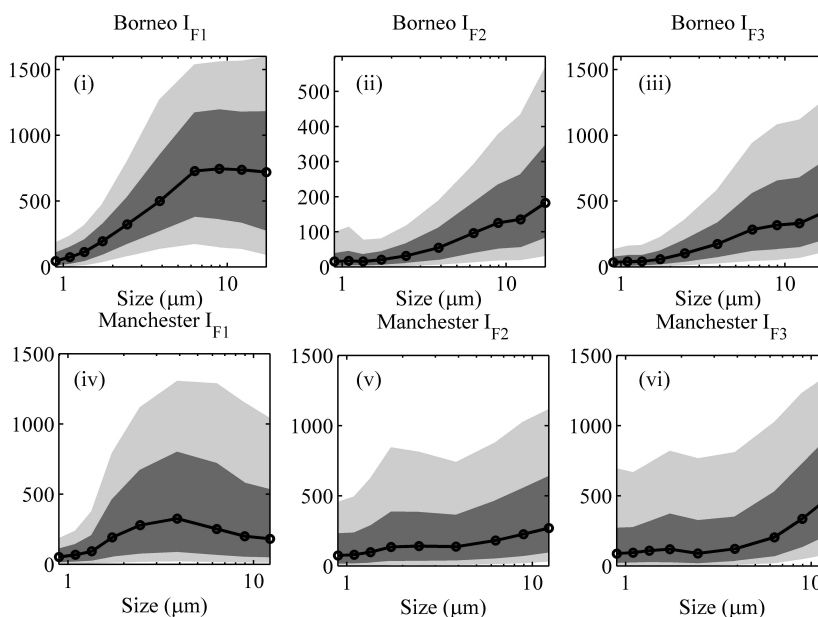


Fig. 8. Fluorescence intensity (arbitrary scale) versus D_p in each WBS3 fluorescence channel in Borneo (upper panel) and Manchester (lower panel). Solid line: median, dark shading: inter-quartile range, light shading: 10 % and 90 %.

rather than absolute fluorescence intensity alone removes particle size effects and effectively compares the relative number of fluorophores in a particle of given D_p .

3.3.1 Correlations between I_{F1} , I_{F2} and I_{F3}

Scatter plots of single-particle fluorescence intensity in each pair of channels (using 2 % of particles randomly selected across each dataset so as not to obscure plot features), coloured by the fluorescence intensity in the other channel are printed in Figs. S5 and S6 for Manchester and Borneo respectively. These illustrate the strong correlation ($r = 0.84$) and linear relationship between I_{F2} and I_{F3} in Manchester and a weaker link between I_{F1} and I_{F2} ($r = 0.21$). In Borneo the degree of correlation is more consistent in each pair of channels, ranging from 0.4 between I_{F1} and I_{F3} to 0.58 between I_{F2} and I_{F3} , and this reflects the broad fluorescence spectrum of fungal spores reported by other work (e.g. Pinnick et al., 1998).

A reduction in the range of I_{F1} values with increasing I_{F3} (a basic proxy for D_p) can also be seen in Manchester, and this is related to the inflexion in Fig. 8iv. In summary, the single-particle data demonstrates that the fluorescence intensities in pairs of WBS3 channels are correlated positively, but the degree of correlation in each pairing varies between sites. This illustrates that while both sites feature contributions of N_{F1} AND 3 and N_{F2} AND 3 the fluorescence intensities within these subsets do not relate to one another in the same way under different local influences.

3.3.2 Size-resolved fluorescence ratios

Intensity ratios are presented in Fig. 9 for each possible permutation of I_{F1} , I_{F2} and I_{F3} at the two sites. This effectively displays the gradients in the scatter plots discussed previously, resolved by D_p . In each case only those particles with non-zero and non-saturating fluorescence intensity in both of the relevant channels are considered and consequently the I_{F2}/I_{F3} plot in Borneo is based on fewer particles than I_{F1}/I_{F3} . This selection process also results in slightly modified I_{F1} , I_{F2} and/or I_{F3} versus D_p curves for each pair of channels used. This modification generally manifests as increased median fluorescence intensity, and the relationships between I and D_p are not systematically different from the general case (Fig. 8) except for small enhancements in I_{F3} and I_{F1} at 0.8–1.5 μm when each is paired with F2 in Borneo. The Manchester I_{F1} inflexion at 4 μm remains present, which leads to the remarkable observation that I_{F1} and I_{F3} diverge with increasing D_p when each particle emits both types of fluorescence. The individual I versus D_p plot associated with each ratio is printed in Fig. S7 (Manchester) and S8 (Borneo) for completeness.

In Borneo I_{F1}/I_{F2} and I_{F1}/I_{F3} (Fig. 9i, ii) are essentially invariant at $D_p \geq 2 \mu\text{m}$, which is consistent with the monotonic relationships in Fig. 8. This suggests one broad type of fluorescent particle (i.e. fungal spores) dominates this size range. The smaller modal ratios at $D_p < 2 \mu\text{m}$ are found in the same size range as enhanced I_{F2} . The change in median I_{F1}/I_{F2} between these size regimes is large compared with the inter-quartile range, indicating a second particle type at $D_p < 2 \mu\text{m}$. The fact that $N_{F1} < N_{F3}$ at $D_p \leq 2 \mu\text{m}$ in

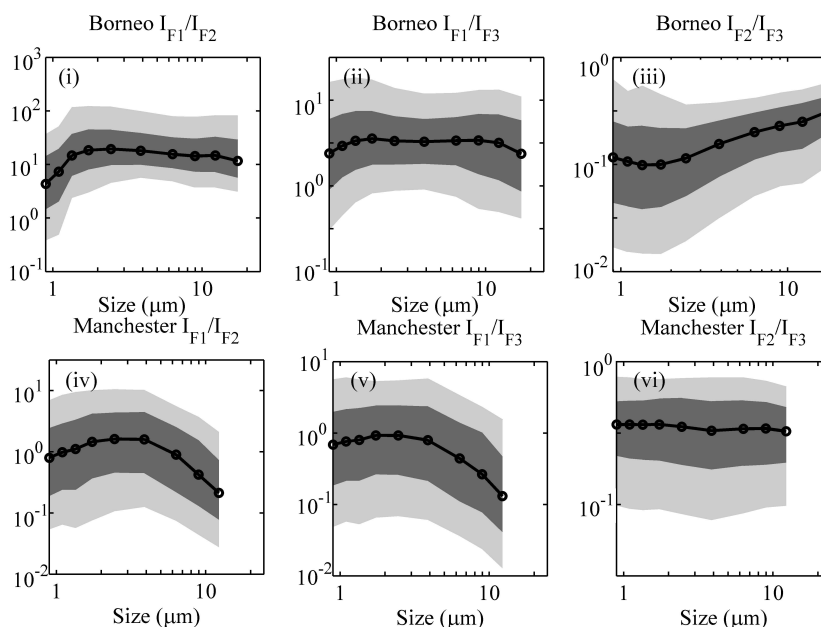


Fig. 9. Size-resolved fluorescence intensity and ratios using each combination of fluorescence channels in Borneo (upper panel) and Manchester (lower panel).

Borneo suggests this second particle type delivers low I_{F1} that is not always detected. Median I_{F2} is less than I_{F3} in Borneo across all size classes, but dI_{F2}/dD_p increases more strongly with D_p . The net result of both is a range of I_{F2}/I_{F3} values spanning 1.5 orders of magnitude at $D_p \leq 2 \mu\text{m}$ followed by an upward trend in the I_{F2}/I_{F3} ratio as size increases (Fig. 9iii).

The Manchester I_{F1}/I_{F2} and I_{F1}/I_{F3} plots (Fig. 9iv, v) vary strongly with D_p and feature large inter-quartile ranges, with the former caused by the relationship between I_{F1} and D_p and the latter by the wide range of fluorescent intensities found at all sizes. In contrast, the I_{F2}/I_{F3} plot (Fig. 9vi) features almost no change with D_p , reflecting the linearity between I_{F2} and I_{F3} in Manchester. The inter-quartile range is also small compared with the other ratios at both sites and indicates that the F2 and F3 channels measure same fluorophore, or fluorophores that scale equally with D_p despite the large range of I_{F2} and I_{F3} at all size intervals being consistent with a mixture of fluorescent “species”. This is distinct from the Borneo case where the relationship is weaker between I_{F2} and I_{F3} .

Given the separation in wavebands between F1 and F3 and the size dependence of the I_{F1}/I_{F2} and I_{F1}/I_{F3} curves in both environments, it appears that the F3 channel measures fluorophores that are largely independent of those detected by F1. The relatively simple aerosol composition in Borneo at $D_p \geq 2 \mu\text{m}$ demonstrates that Tryptophan and NAD(P)H density is the same in this size range, hence their common scaling with D_p . The consistent I_{F2}/I_{F3} versus D_p relationship observed in Manchester compared with Borneo, and vice-versa for I_{F1}/I_{F3} and I_{F1}/I_{F2} in Borneo compared with

Manchester, may be useful qualitative comparisons when analysing fluorescence data recorded using multiple wavelength excitation and detection.

Diagnostic data and the measured response of the WIBS3 to various calibration media over time suggest that negligible drift, if any, has occurred in the fluorescence excitation/detection channel calibrations and therefore the two datasets are likely to be directly comparable. As such, the limited overlap between the inter-quartile ranges of I_{F1}/I_{F3} in Manchester and Borneo allows some degree of distinction to be made between the sites in a way that includes the largest number of fluorescent aerosol in Borneo. The dependence of the various fluorescence intensity metrics on D_p discussed here would still be noteworthy even in the event of calibrations having changed, but the specific values of the ratios and fluorescence intensities would not be comparable. The reason for the specific value of each ratio is not known but is likely a product of the fluorescence quantum yield of different fluorophores, the presence of interferents and absorbing material, or the way in which the fluorescent material is arranged inside the aerosol particle affects extinction at UV or visible wavelengths.

4 Further discussion

With typical values of $0\text{--}3001^{-1}$, the urban fluorescent particle concentration is comparable to that of bacteria measured in Birmingham, UK, in the winter by Harrison et al. (2005). The dominance of N_{F3} over N_{F1} is not consistent with published laboratory measurements of bacteria fluorescence,

which suggest stronger F1 fluorescence than F3 would be present if bacteria dominated the fluorescent aerosol. The diurnal concentration variation in Manchester appears partly linked to traffic activity, which can respectively increase airborne PBA and fluorescent non-PBA number through re-suspension of both and primary PAH production. Ambient measurements by Pinnick et al. (2004) using a 266 nm excitation found the number fractions of fluorescent particles corresponding to N_{F1} and N_{F2} ($3 \leq D_A \leq 10 \mu\text{m}$) were similar in an urban environment, as observed here, but the majority of fluorescent aerosol appeared to be non-PBA based on the wavelength-dispersed fluorescence spectra. As a result of these factors and the limited PBA abundance in filter samples, neither PBA nor false-positives can be ruled out as the dominant fluorescent aerosol component in Manchester in this study, and measurements in remote locations may provide some insight into the urban contribution to each fluorescent number concentration.

The measurements using channel F3 are comparable to UV-APS measurements performed by Huffman et al. (2010) and Pöschl et al. (2010) in Mainz, Germany, and Amazonia, respectively. The similarity between the WIBS3 and UV-APS fluorescent size spectra are remarkable in light of the different particle sizing methods used. Pöschl et al. find a 1.5–3 μm fluorescent size mode similar to that in Borneo, and also determine that it is dominated by PBA using SEM images and elemental analysis. Huffman et al. detect fluorescent size modes at $D_A \leq 1 \mu\text{m}$ and at 2–4 μm , and conclude that 25 % of the aerosol larger than 4 μm is likely to be fluorescent biological aerosol. The Manchester N_{F3} size spectrum (Fig. 4iv) contains similar size modes and a comparable relationship between fluorescent number fraction and particle size, albeit with larger values. Huffman et al. attribute the smaller size mode to PAHs confined to this size range, however the ESEM images obtained in Manchester (Fig. S9) show that soot is readily found with characteristic size up to 10 μm and the same assumption cannot be made for Manchester.

A potential use for the fluorescence ratio data from Borneo is as a set of upper and lower thresholds to identify similar material in a low-PBA environment, since it captures the broad fluorescence characteristics of fungal spores, which are surprisingly consistent. To demonstrate this, the Manchester dataset was limited to those particles with I_{F1}/I_{F3} within the inter-quartile range in each D_P bin in Borneo. The F1 and F3 pairing was chosen because it captures the most fluorescent particles in Borneo. The typical resulting concentration of “Borneo-like” particles in Manchester was $2\text{--}191^{-1}$ (10th and 90th percentiles) compared with corresponding $N_{F1 \text{ AND } 3}$ of $6\text{--}711^{-1}$ in Manchester. Both products contain size modes at 0.8–1.2 μm and 2–3 μm and this result demonstrates the “fine-tuning” of the initial analysis (concerning the presence of fluorescence in one or more channels) that can be achieved. The similarity of the resulting size distribution to the general Manchester case, however, illustrates the

difficulty in stating whether this represents the fungal spore concentration within the Manchester aerosol, or whether it is simply a consequence of the large range of fluorescence ratios found there.

5 Summary

WIBS3 data was collected in the winter in Manchester and below the canopy of tropical rainforest in Borneo, Malaysia. Previous studies of urban PBA and fluorescent aerosol and in-situ ESEM/EDX data suggest the fluorescent aerosol is more likely to feature non-PBA in Manchester than in Borneo. The two datasets are therefore taken to reflect fluorescent aerosol with a weak PBA influence and strong PBA influence (based on previously published work), respectively.

The concentration and size distributions of fluorescent aerosol in each WIBS3 channel vary significantly between Manchester and Borneo, with consistent size spectra in each channel at a particular site. In Manchester fluorescent particles number $0\text{--}3001^{-1}$ whereas in Borneo they number $100\text{--}20001^{-1}$. Fluorescent aerosol size distributions contain primary modes at 0.8–1.2 μm in Manchester and at 3–4 μm in Borneo.

Fluorescent aerosol in Manchester represented 11 % or less of N_{TOT} in the WIBS3 size range (0.8–20 μm). In Borneo the majority of fluorescent aerosol was sized 3–4 μm and represented up to 66 % of N_{TOT} over the whole WIBS3 size range. The size-resolved fluorescence intensity and ratios of fluorescence intensity in different combinations of channels were compared, and their relationships with particle size were found to differ between the sites in every case. The intensity in fluorescence detection channels F2 and F3 were found to vary approximately linearly with D_P at both sites rather than with D_P^2 , and this may represent the diversity of fluorescent sub-species found at each site that cannot be resolved specifically using this technique. The results obtained in Borneo were used to constrain the Manchester dataset and a “Borneo-like” particle concentration was derived.

6 Conclusions

This work demonstrates that the ensemble aerosol at an urban and a tropical rainforest site can be partially distinguished based on the size distributions of particles fluorescent at 400–600 nm after a 350 nm excitation (channel F3), and this is consistent with previous studies. Additional discrimination is provided by monitoring fluorescence at 310–400 nm after a 280 nm excitation (channel F1), which appears more selective than the 350 nm excitation at the urban site.

The PBA-dominated fluorescent size distributions in Borneo peak at 2–3 μm whereas in the urban case, which is likely to feature more fluorescent non-PBA, they contain characteristic size modes at 0.8–1.2 μm with secondary features at

2–4 μm . N_{F3} consistently outnumbers N_{F1} by a factor of 2–3 across the urban size spectrum, both in this campaign and subsequent measurements in Manchester, whereas in Borneo they are comparable throughout. The magnitude of this difference is concluded to be a feature of the urban fluorescent aerosol, each component of which peaks in concentration in the mid-morning during elevated N_{NON} , and may be related to rush-hour traffic.

A D_{P} -invariant I_{F2}/I_{F3} ratio in Manchester is caused by a linear relationship between the two fluorescence intensities, which is not the case in Borneo. The converse is true of I_{F1}/I_{F3} , which are more strongly related in Borneo than in Manchester at $D_{\text{P}} > 2 \mu\text{m}$. This indicates consistent proportions of Tryptophan and NAD(P)H in fungal spore material, and of the unidentified fluorophores detected by the F2 and F3 channels in urban aerosol. These features therefore distinguish the ensemble fluorescent aerosol in the two environments, but do not provide absolute discrimination. This way of combining WBS3 metrics retains D_{P} as an independent degree of freedom, simplifying its interpretation.

Size-resolved I_{F1}/I_{F3} data was used to select “Borneo-like” particles in Manchester, which resulted in a median concentration of 101^{-1} . This is around half of $N_{F1 \text{ AND } 3}$ in Manchester and demonstrates a complementary selection technique to the approach used in Gabey et al. (2010) that involves the presence of fluorescence in multiple channels to provide a basic classification scheme, however it does not unambiguously represent PBA.

Supplementary material related to this article is available online at:
<http://www.atmos-chem-phys.net/11/5491/2011/acp-11-5491-2011-supplement.pdf>

Acknowledgements. This work was funded by the Natural Environment Research funded projects “Aerosol Characterisation Experiment” (ACES) (contract # NE/E011233/1), part of the NERC APPRAISE programme (Aerosol Properties, Processes And Influences on the Earth’s Climate), and the NERC Oxidant & Particle Photochemical Processes Tropical Rain Forest (OP3) project contract # NE/D004624/1. We thank the Malaysian and Sabah Governments for their support; the Malaysian Meteorological Department (MMD) for access to the Bukit Atur Global Atmosphere Watch station; W. Sinun of Yayasan Sabah and his staff; and G. Reynolds of the Royal Society’s South East Asian Rain Forest Research Programme and his staff for logistical support at the Danum Valley Field Centre. Mr. Gabey is in receipt of a NERC studentship. Thanks are also due to R. Burgess, Centre for Atmospheric Science, Manchester, for her assistance with the ESEM analysis.

Edited by: Y. Rudich

References

- Agranovski, V., Ristovski, Z., Hargreaves, M., Blackall, P. J., and Morawska, L.: Real-time measurement of bacterial aerosols with the UVAPS: Performance evaluation, *J. Aerosol Sci.*, 34, 301–317, 2003a.
- Agranovski, V., Ristovski, Z., Hargreaves, M., J. Blackall, P., and Morawska, L.: Performance evaluation of the UVAPS: influence of physiological age of airborne bacteria and bacterial stress, *J. Aerosol Sci.*, 34, 1711–1727, 2003b.
- Bauer, H., Kasper-Giebl, A., Löflund, M., Giebl, H., Hitznerberger, R., Zibuschka, F., and Puxbaum, H.: The contribution of bacteria and fungal spores to the organic carbon content of cloud water, precipitation and aerosols, *Atmos. Res.*, 64, 109–119, 2002.
- Diehl, K., Quick, C., Matthias-Maser, S., Mitra, S. K., and Jaenicke, R.: The ice nucleating ability of pollen: Part I: Laboratory studies in deposition and condensation freezing modes, *Atmos. Res.*, 58, 75–87, 2001.
- Diehl, K., Matthias-Maser, S., Jaenicke, R., and Mitra, S. K.: The ice nucleating ability of pollen: Part II. Laboratory studies in immersion and contact freezing modes, *Atmos. Res.*, 61, 125–133, 2002.
- Elbert, W., Taylor, P. E., Andreae, M. O., and Pöschl, U.: Contribution of fungi to primary biogenic aerosols in the atmosphere: wet and dry discharged spores, carbohydrates, and inorganic ions, *Atmos. Chem. Phys.*, 7, 4569–4588, doi:10.5194/acp-7-4569-2007, 2007.
- Faris, G. W., Copeland, R. A., Mortelmans, K., and Bronk, B. V.: Spectrally resolved absolute fluorescence cross sections for bacillus spores, *Appl. Opt.*, 36, 958–967, 1997.
- Foot, V. E., Kaye, P. H., Stanley, W. R., Barrington, S. J., Gallagher, M., and Gabey, A.: Low-cost real-time multiparameter bio-aerosol sensors, *Optically Based Biological and Chemical Detection for Defence IV*, Cardiff, Wales, United Kingdom, 71160I-71112, 2008.
- Gabey, A. M., Gallagher, M. W., Whitehead, J., Dorsey, J. R., Kaye, P. H., and Stanley, W. R.: Measurements and comparison of primary biological aerosol above and below a tropical forest canopy using a dual channel fluorescence spectrometer, *Atmos. Chem. Phys.*, 10, 4453–4466, doi:10.5194/acp-10-4453-2010, 2010.
- Gilbert, G. S. and Reynolds, D. R.: Nocturnal Fungi: Airborne Spores in the Canopy and Understory of a Tropical Rain Forest, *Biotropica*, 37, 462–464, 2005.
- Harrison, R. M., Jones, A. M., and Lawrence, R. G.: Major component composition of PM_{10} and $\text{PM}_{2.5}$ from roadside and urban background sites, *Atmos. Environ.*, 38, 4531–4538, 2004.
- Harrison, R. M., Jones, A. M., Biggins, P. D. E., Pomeroy, N., Cox, C. S., Kidd, S. P., Hobman, J. L., Brown, N. L., and Beswick, A.: Climate factors influencing bacterial count in background air samples, *Int. J. Biometeorol.*, 49, 167–178, 2005.
- Hewitt, C. N., Lee, J. D., MacKenzie, A. R., Barkley, M. P., Carslaw, N., Carver, G. D., Chappell, N. A., Coe, H., Collier, C., Commane, R., Davies, F., Davison, B., DiCarlo, P., Di Marco, C. F., Dorsey, J. R., Edwards, P. M., Evans, M. J., Fowler, D., Furneaux, K. L., Gallagher, M., Guenther, A., Heard, D. E., Helfter, C., Hopkins, J., Ingham, T., Irwin, M., Jones, C., Karunaharan, A., Langford, B., Lewis, A. C., Lim, S. F., MacDonald, S. M., Mahajan, A. S., Malpass, S., McFiggans, G., Mills, G., Misztal, P., Moller, S., Monks, P. S., Nemitz, E., Nicolas-Perea, V., Oetjen, H., Oram, D. E., Palmer, P. I.,

- Phillips, G. J., Pike, R., Plane, J. M. C., Pugh, T., Pyle, J. A., Reeves, C. E., Robinson, N. H., Stewart, D., Stone, D., Whalley, L. K., and Yin, X.: Overview: oxidant and particle photochemical processes above a south-east Asian tropical rainforest (the OP3 project): introduction, rationale, location characteristics and tools, *Atmos. Chem. Phys.*, 10, 169–199, doi:10.5194/acp-10-169-2010, 2010.
- Hill, S. C., Pinnick, R. G., Niles, S., Fell, N. F., Pan, Y.-L., Bottiger, J., Bronk, B. V., Holler, S., and Chang, R. K.: Fluorescence from Airborne Microparticles: Dependence on Size, Concentration of Fluorophores, and Illumination Intensity, *Appl. Opt.*, 40, 3005–3013, 2001.
- Hill, S. C., Mayo, M. W., and Chang, R. K.: Fluorescence of Bacteria, Pollens, and Naturally Occurring Airborne Particles: Excitation/Emission Spectra, Army Research Laboratory, 2009.
- Ho, J.: Real time detection of biological aerosols with fluorescence aerodynamic particle sizer (FLAPS), *J. Aerosol Sci.*, 27, 581–582, 1996.
- Huffman, J. A., Treutlein, B., and Pöschl, U.: Fluorescent biological aerosol particle concentrations and size distributions measured with an Ultraviolet Aerodynamic Particle Sizer (UV-APS) in Central Europe, *Atmos. Chem. Phys.*, 10, 3215–3233, doi:10.5194/acp-10-3215-2010, 2010.
- Kaye, P., Stanley, W. R., Hirst, E., Foot, E. V., Baxter, K. L., and Barrington, S. J.: Single particle multichannel bio-aerosol fluorescence sensor, *Opt. Express*, 13, 3583–3593, 2005.
- Lakowicz, J. R.: Principles of fluorescence spectroscopy, 3rd Edition, Springer, New York, 2006.
- Matthias-Maser, S. and Jaenicke, R.: The size distribution of primary biological aerosol particles with radii $>0.2 \mu\text{m}$ in an urban/rural influenced region, *Atmos. Res.*, 39, 279–286, 1995.
- Pan, Y.-L., Pinnick, R. G., Hill, S. C., Rosen, J. M., and Chang, R. K.: Single-particle laser-induced-fluorescence spectra of biological and other organic-carbon aerosols in the atmosphere: Measurements at New Haven, Connecticut, and Las Cruces, New Mexico, *J. Geophys. Res.*, 112, D24S19, doi:10.1029/2007JD008741, 2007.
- Pan, Y.-L., Hill, S. C., Pinnick, R. G., Huang, H., Bottiger, J. R., and Chang, R. K.: Fluorescence spectra of atmospheric aerosol particles measured using one or two excitation wavelengths: Comparison of classification schemes employing different emission and scattering results, *Opt. Express*, 18, 12436–12457, 2010.
- Pan, Y.-L., Hill, S. C., Pinnick, R. G., House, J. M., Flagan, R. C., and Chang, R. K.: Dual-excitation-wavelength fluorescence spectra and elastic scattering for differentiation of single airborne pollen and fungal particles, *Atmos. Environ.*, 45, 1555–1563, 2011.
- Pinnick, R. G., Hill, S. C., Nachman, P., Videen, G., Chen, G., and Chang, R. K.: Aerosol Fluorescence Spectrum Analyzer for Rapid Measurement of Single Micrometer-Sized Airborne Biological Particles, *Aerosol Sci. Technol.*, 28, 95–104, 1998.
- Pinnick, R. G., Hill, S. C., Pan, Y.-L., and Chang, R. K.: Fluorescence spectra of atmospheric aerosol at Adelphi, Maryland, USA: measurement and classification of single particles containing organic carbon, *Atmos. Environ.*, 38, 1657–1672, 2004.
- Pöschl, U., Martin, S. T., Sinha, B., Chen, Q., Gunthe, S. S., Huffman, J. A., Borrmann, S., Farmer, D. K., Garland, R. M., Helas, G., Jimenez, J. L., King, S. M., Manzi, A., Mikhailov, E., Pauliquevis, T., Petters, M. D., Prenni, A. J., Roldin, P., Rose, D., Schneider, J., Su, H., Zorn, S. R., Artaxo, P., and Andreae, M. O.: Rainforest Aerosols as Biogenic Nuclei of Clouds and Precipitation in the Amazon, *Science*, 329, 1513–1516, doi:10.1126/science.1191056, 2010.
- Schauer, C., Niessner, R., and Pöschl, U.: Analysis of nitrated polycyclic aromatic hydrocarbons by liquid chromatography with fluorescence and mass spectrometry detection: air particulate matter, soot, and reaction product studies, *Anal. Bioanal. Chem.*, 378, 725–736, 2004.
- Sivaprakasam, V., Huston, A., Scotto, C., and Eversole, J.: Multiple UV wavelength excitation and fluorescence of bioaerosols, *Opt. Express*, 12, 4457–4466, 2004.
- Sivaprakasam, V., Huston, A., Lin, H. B., Eversole, J., Falkenstein, P., and Schultz, A.: Field test results and ambient aerosol measurements using dual wavelength fluorescence excitation and elastic scatter for bioaerosols, Chemical and Biological Sensing VIII, Orlando, FL, USA, 65540R-65547, 2007.
- Uk Lee, B., Jung, J. H., Yun, S. H., Hwang, G. B., and Bae, G. N.: Application of UVAPS to real-time detection of inactivation of fungal bioaerosols due to thermal energy, *J. Aerosol Sci.*, 41, 694–701, 2010.
- Westphal, A. J., Price, P. B., Leighton, T. J., and Wheeler, K. E.: Kinetics of size changes of individual *Bacillus thuringiensis* spores in response to changes in relative humidity, *P. Natl. Acad. Sci. USA*, 100, 3461–3466, doi:10.1073/pnas.232710999, 2003.
- Yarwood, C. E.: Water Content of Fungus Spores, *American Journal of Botany*, 37, 636–639, 1950.